Solar Energy Materials and Solar Cells xxx (xxxx) xxx–xxx

Contents lists available at ScienceDirect

Solar Energy Materials and Solar Cells

journal homepage: www.elsevier.com/locate/solmat

On the origin of band-tails in kesterite

G. Rey[a,*], G. Larramona[b], S. Bourdais[b], C. Choné[b], B. Delatouche[b], A. Jacob[b], G. Dennler[b], S. Siebentritt[a]

[a] Laboratory for Photovoltaics (LPV), Physics and Materials Science Research Unit, 41 rue du Brill, L-4422 Belvaux, Luxembourg
[b] IMRA Europe S.A.S., 220 rue Albert Caquot, 06904 Sophia Antipolis, France

ARTICLE INFO

Keywords:
Kesterite
Band-tail
Photoluminescence
CZTSe
CZTSSe

ABSTRACT

Kesterite $Cu_2ZnSn(S_xSe_{1-x})_4$ is an attractive earth-abundant material for low-cost thin film photovoltaics with the capability to achieve power production in the terawatt range and therefore to supply a significant part of the global electricity needs. Despite its advantageous optical and electrical properties for photovoltaic applications, the large band tailing causes voltage losses that limit the efficiency of kesterite-based devices. Here we show that the band-tailing originates mainly from band-gap fluctuations attributable to chemical composition variations at nanoscale; while electrostatic fluctuations play a lesser role. Absorption measurement reveal that the Cu-Zn disorder, always present in kesterite $Cu_2ZnSn(S_xSe_{1-x})_4$, is not the main source of the large band tailing. Instead defect clusters having a significant impact on the band-edge energies, e.g. $[2Cu_{Zn}^{-} + Sn_{Zn}^{2+}]$, are proposed as the main origin for the kesterite band tail.

1. Introduction

Photovoltaics (PV) provides already more than 1% of the global electricity production, with 7–8% in some countries and with a worldwide increasing trend [1]. Cost-competitiveness is the most important criterion to ensure further extensive PV deployment. This translates to the need of low-cost, large-scale and high throughput PV technology, ideally based on earth-abundant and non-toxic material. Kesterite materials, $Cu_2ZnSn(S_xSe_{1-x})_4$ (CZTSSe), has been seen as promising semiconductor for PV [2–4], taking advantage of the large abundance of its metallic constituents, of its direct band-gap [5], adjustable in the 1–1.5 eV range by sulfo-selenide alloying [6–8] leading to intense solar light absorption [9], of favourable transport and doping behaviour [10,11] and of the possibility to grow this semiconductor with large grain at moderate temperature [12]. These properties allowed to achieve solar cells with power conversion efficiencies close to 13% [13]. However, in comparison to other thin-film PV technologies i.e. CIGS (best efficiencies 22.6% [14]) and CdTe (22.1% [15]), kesterite-based PV still shows lower conversion efficiencies limited by both open-circuit voltage (V_{oc}) and fill factor [4,16,17]. Thus, it is essential to understand: what is the main source of recombination to further improve the efficiency of kesterite solar cells. Several mechanisms might be responsible for the increased recombination of kesterite-based devices: those related to the hetero-junction partner and buffer [18,19], to non-ohmic contacts [20,21], grain-boundaries [22,23] or secondary phases [24]. However, the most fundamental loss mechanisms are related to the intrinsic properties of kesterite bulk: due to native deep defects acting as recombination centres [25] or the presence of band-tails [26], limiting the useful energy of photo-generated carriers and their transport. It has been argued that tail states reduce the open circuit voltage only slightly. However, this is only true in the case where radiative recombination is the dominating recombination path [27], whereas tail states also contribute to Shockley-Read-Hall recombination [28], thereby further reducing the room temperature V_{oc} [29].

Tail states are caused by two known fundamental mechanisms [4,30]: either a high concentration of defects combined with a high degree of compensation, which cause the electrostatic potential to fluctuate; or crystalline or compositional inhomogeneities which cause the band-edges and consequently the band-gap to fluctuate.

A potential cause for band-gap fluctuations and electrostatic potential fluctuations in kesterite is the occurrence of Cu-Zn disorder [31,32]. The kesterite material undergoes a Cu-Zn order-disorder transition which is a second order transition. As depicted in Fig. 1, under thermal excitation, Cu and Zn atoms, located in the planes at $z = \frac{1}{4}$ and $\frac{3}{4}$ in the unit cell, can exchange position at low energy cost [25,33–35], because of the similar size of the cations. Therefore, the critical temperatures T_c of the transition are low i.e. 200 °C for pure selenide kesterite (CZTSe) [36] or Se-rich CZTSSe [37] and 260 °C for pure sulphide [31,38]. On the one hand, the band-gap of the material

* Corresponding author.
E-mail address: germrey@gmail.com (G. Rey).
URL: http://www.germain.rey@uni.lu (G. Rey).

https://doi.org/10.1016/j.solmat.2017.11.005
Received 18 July 2017; Received in revised form 9 October 2017; Accepted 3 November 2017

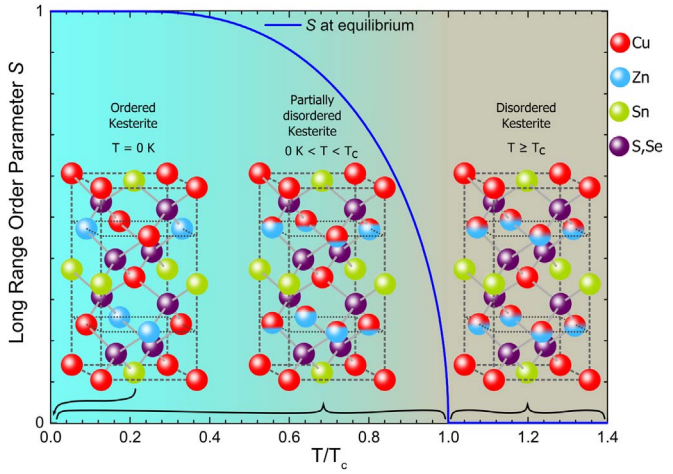

Fig. 1. Illustration of the ordered, Cu-Zn partially ordered and Cu-Zn fully disordered kesterite structure. The plot shows the evolution of the long range order parameter (S) at equilibrium versus the reduced temperature ($\frac{T}{T_c}$) as given by the Bragg and Williams equation $S = \tanh(ST_c/T)$ [42].

depends on the Cu-Zn order state [36,39] and may induce band-gap fluctuations. On the other hand, it is theoretically predicted that Cu_3SnS and $CuZn_2SnS$ S-centred tetrahedral motifs, resulting from Cu-Zn disorder, can cluster in charged nanodomains leading to band-tails induced by fluctuating electrostatic potential [33]. Also clusters of Zn^{+}_{Cu} antisites have been observed by scanning transmission electron microscopy [40].

Although the effects of the Cu-Zn disorder on the crystalline structure, band-gap energy and vibrational properties are well documented, its real impact on the band-tail is still not clarified. The question therefore arises: is the Cu-Zn disorder the main responsible for the large kesterite band tailing? That question has serious implications for the interest in kesterite for PV. Because of the low critical temperature of the Cu-Zn order-disorder transition, kesterite materials always show a significant Cu-Zn disorder [41]. Consequently, it would be an intrinsic limitation of the material if the band tails would mainly result from the Cu-Zn disorder.

In the present work, we investigate the origin of the band tailing in kesterite. First, we determine the nature of the fluctuation that are responsible for the large band tailing in kesterite, which is yet not clarified [43], by investigating the photoluminescence (PL) versus temperature and excitation intensity of high quality CZTSSe (leading to solar cell efficiency above 9%). The behaviour of the spectral broadening with excitation intensity at low temperature (6 K) points out band-gap fluctuations, as opposed to electrostatic potential fluctuations, as the most important cause of the band tailing in kesterite. Therefore, we measure the absorption coefficient (α) spectrum of CZTSSe and CZTSe by spectrophotometry (SP) and PL to be able to measure band tail induced absorption with a high dynamic range. Identical kesterite samples were thermally treated either to induce Cu-Zn disorder or to reduce the Cu-Zn disorder. The comparison of absorption spectra did not reveal any differences in terms of band tailing for Cu-Zn disordered kesterite and partially Cu-Zn ordered kesterite despite the effort in reaching high degree of Cu-Zn order. Both investigations tend to confirm that the large kesterite band tails do not result directly from band-gap variation due to the Cu-Zn disorder.

2. Experimental details

2.1. Sample preparation and post-treatment

CZTSe samples were deposited on Mo-coated soda lime glass substrates heated at 470 °C by co-evaporation of Cu, Zn, Sn, SnSe and Se in a molecular beam epitaxy system. The co-evaporation process was divided in two main steps: first all elements were supplied to form the kesterite, then only Sn, SnSe and Se were supplied to improve crystal quality and prevent Sn- and Se-loss. The samples were terminated with a Zn-rich surface. Se was supplied during final cool-down down to 200 °C. This co-evaporation process is detailed in Ref. [44]. The film composition determined by energy-dispersive X-ray spectroscopy was Cu-poor and Zn-rich (CZTSe#1: Cu/(Zn + Sn) = 0.82, Zn/Sn = 1.10 and CZTSe#2: Cu/(Zn + Sn) = 0.87, Zn/Sn = 1.15).

CZTSSe samples were fabricated as follows. CZTS layers were deposited on Mo glass substrates by non-pyrolytic spraying inside a N_2-filled glove box, using an additive-free water-ethanol (90–10 vol%) based ink of a Cu-Zn-Sn sulphide (no Se) colloid of ~ 10 nm size primary particles, as described in Ref. [45]. The as-sprayed films were submitted to a two-step annealing process: a first annealing step in inert (N_2) atmosphere, allowing to grow the precursor particles from nanometer up to micrometer size, and a second annealing step in Se vapor containing atmosphere allowing both the incorporation of Se (replacing the S) and the curing of the secondary phases present after the first annealing step, as described in Ref. [46]. The Se content of the films was around 60–70% atomic of the total amount (S + Se). The Cu/Zn/Sn ratio in the metal precursors was off-stoichiometric: 1.7/1.1/1 for the CZTSSe#1 and CZTSSe#3 series, 1.9/1.2/1 for the CZTSSe#2 series.

For CZTSe#1 samples, the optional post-synthesis treatments were carried out in a tube furnace filled with N_2 at atmospheric pressure. For CZTSSe samples and CZTSe#2 samples, the optional post-synthesis treatments were performed on a hot plate inside a N_2-filled glove box. The thermal quenching was carried out either by transferring the sample to a cold part of the tube furnace and actively cooling under N_2 flux at room temperature or by transferring the samples from the hot plate to a room temperature holder

2.2. Material characterisation

To perform normal incidence transmittance ($\mathscr{T}$) and 8° incidence reflectance ($\mathscr{R}$) measurements, kesterite thin films were mechanically transferred on glass or quartz substrate using transparent epoxy. The transmittance and reflectance were measured with an UV–vis–NIR dual beam spectrophotometer equipped with a 150 mm integrating sphere. $\mathscr{T}$ and $\mathscr{R}$ were analysed in the framework of the transfer matrix method to extract the complex refractive index ($n + ik$).

Temperature and intensity dependent PL measurement were conducted on a standard CZTSSe#1 sample (neither ordering treatment or disordering treatment) covered with CdS. The sample was placed in a continuous flow cryostat cooled with helium in which the temperature was controlled by a heating stage. A 660 nm diode laser was used for sample excitation. The laser light went through a narrow band-pass filter and a short-pass filter to remove laser harmonics. The excitation was varied by adjusting the laser power (1–100 mW) and using optional calibrated grey filters (OD1-OD4). The laser light was focused on the sample in a 0.1 mm radius spot using a lens. The PL signal was collected by parabolic mirrors. The collected light went through an 850 nm long-pass filter to remove laser reflection and the intensity of the PL signal was optionally attenuated using an OD2 calibrated grey filter. The PL signal was measured by a monochromator coupled with an InGaAs camera. The spectral response of the system was corrected using a calibrated reference lamp. Some measurement artefacts might be seen in the PL spectra due to water absorption around 0.9 eV.

The absorption coefficient measurements by PL, were done on samples prepared similarly as for spectrophotometry measurements (except for the CZTSe#1 series where the PL was measured on thin films deposited Mo-coated glass and covered with CdS). The PL system is the same as described previously except that the laser light was not focused using a lens to obtain a laser spot larger than the PL signal collection area such that the illumination can be considered homogeneous within the sample part from which the PL signal is recorded. In

addition, the laser photon flux was measured at the sample position using a powermetre. Besides the spectral correction, an intensity correction factor was determined from the laser reflection on a Spectralon standard in order to obtain the absolute PL yield. The absorption coefficient was obtained from the absolute PL spectra [47]. For a thin film on a substrate, the equation given in Ref. [47] has to be modified to account for different light behaviour at the front and at the back which was included by using the transfer matrix method in the same framework used for spectrophotometry evaluation as described in Supplementary material.

3. Results

3.1. Potential fluctuation in kesterites

We use temperature and excitation intensity dependent PL measurements to evaluate the origin of the band-tails in CZTSSe. For all temperatures and excitation intensities investigated here, the PL signal consists of broad asymmetric peak[1] as seen in Fig. 2a and b with a stretched low-energy side which reflects the joint density of states [48]. The steeper high-energy slope depends on the carrier distribution and thus, in the case of distorted bands, on how the photogenerated carriers can move between neighbouring energy extrema. The peak maximum position and peak maximum intensity are reported in Fig. 2c and d. At 150 K and at lower temperatures, the cooling capability of the cryostat was overcome by laser induced heating for the three highest excitation intensities. The increase in temperature is seen in a change of the high energy slope of the PL spectra (Fig. 2a) and induced the downward bending of the low-temperature curves seen in Fig. 2c and d for the three highest excitations.

At low temperature, the PL peak maximum strongly blue-shifts when the laser intensity is increased (15 meV per decade of excitation at 6 K and 50 K) and red-shifts when the temperature is increased. This behaviour is typically encountered in strongly compensated semiconductors [49] and is generally attributed to quasi-donor acceptor pair (QDAP) [49–52] or potential fluctuation [53–56]. Both modelles describe the behaviour of PL emissions under the influence of electrostatic potential fluctuations caused by a high density of compensated defects. Alternatively, band-gap energy fluctuation can also explain such PL behaviour [57,16]. Which of the two mechanisms prevail, is still not clear for kesterite [43].

The blue-shift seen under increased excitation at low temperature can be explained as follow, depending on the origin of the band fluctuation. For electrostatic fluctuations, photogenerated carriers will screen the fluctuating potential and thus reduce the width of the energy level distribution and flatten the distortion. The energy of the occupied state is shifted towards the centre of the fluctuation distribution, leading to a blue-shit. For both electrostatic and/or for band-gap fluctuations, photogenerated carriers fill local minimum energy states. The extra carriers, generated by an increase in excitation will populate empty states which have higher energy than the already filled states leading to a blue-shift of the PL. At low temperature, the red-shift with increasing temperature is related to an increase in carrier mobility. With increasing temperature, the photogenerated carriers can overcome the potential barriers and are redistributed to lower energy states inducing a red-shift of the PL. Alternatively more mobile photogenerated carriers can reach non-radiative recombination centres. Because of the high recombination rate of these centres, the life-time decreases with increased temperature [16], which decreases the photogenerated carrier density. In that case increasing the temperature has a similar effect as to reduce the power excitation, which also leads to a red-shift of the PL.

[1] Although, the PL peak may result from several contributions for the intermediate temperatures and room temperature.

The mechanisms responsible for the PL emission were identified by looking at the relationship between excitation ϕ_l and PL signal I_{pl}: $I_{pl} = \phi_l^k$ [58,59] (see Supplementary materials). For 6 K and 50 K the k-exponent varies from 1 to 0.5 with excitation and PL emission is attributed to a tail-to-impurity transition (TI) (see Supplementary materials). Looking at Fig. 2b, the TI dominates at low temperature whereas for 200 K and above a new band appear at 1–1.05 eV when temperature is rising. From the energy difference between the band gap and the PL peak position and from the k-exponent of 1.3, we assign this emission occurring at higher energy to a band-tail-to-band-tail recombination (TT). The electronic structure is in accordance with the picture drawn from PL and admittance spectroscopy [60]. The transition from TI to TT as main contribution to the PL with increased temperature leads to a blue-shift of the peak position seen in Fig. 2b for $T > 200$ K. At fixed intermediate temperature where TT and TI both significantly affect the peak maximum position, increasing the excitation will increase the relative contribution of TT, which leads to stronger blue-shift than the one observed at low temperature but is not related to stronger fluctuations.

In order to shed some light on the nature of fluctuations, we analysed the low-energy side of the PL as it reflects the density of states affected by the depth of the fluctuations. The low-energy side of the PL peak was fitted by means of a Gaussian function [61] and its standard deviation is reported in Fig. 2e. Here we identify directly the fitted standard deviation to the root mean square depth of the band-edges potential fluctuation γ, although the former accounts only for the states involved in the radiative processes and therefore its value is not strictly equal to γ.

In the case of highly compensated semiconductors, the root mean square depth of the electrostatic fluctuation γ_{el} can be approximated by [62,63]:

$$\gamma_{el} = \frac{e^2}{4\pi\varepsilon_r\varepsilon_0}\frac{N_I^{\frac{2}{3}}}{p^{\frac{1}{3}}} \tag{1}$$

where e is the elementary charge, $\varepsilon_r\varepsilon_0$ is the static permittivity of the semiconductor, N_I is the total charged impurity concentration (i.e. ionised donors + ionised acceptors) and p is the concentration of mobile carriers. Under illumination, N_I is nearly constant at low temperature for highly compensated semiconductor and the carrier concentration can be rewritten as $p = p' + \Delta p + \Delta n$, with p' being the carrier density due to net doping. Δp and Δn being the photogenerated carrier densities for which we assume $\Delta p = \Delta n$. The PL intensity I_{pl} is proportional to the product of the carrier densities: $I_{pl} = b(p' + \Delta p)\Delta n$, neglecting the density of thermally excited electron, b being a proportionality constant.

It is important to stress that γ_{el} given in Eq. (1) as defined in Ref. [62] only accounts for the fluctuation of an electrostatic nature. In addition fluctuation of the band-edges potential can arise, without electrostatic fluctuation, from inhomogeneous material composition leading to electron affinity fluctuation or band-gap energy fluctuation (e.g. different S/Se ratio). Electron affinity fluctuations can be flattened by variation of the electrostatic potential and are also described by Eq. (1), while band-gap energy fluctuation cannot be reduced by change in the electrostatic potential. The contribution of the band-gap fluctuation to the rms depth γ_{bg} is assumed to be independent of the illumination.

When band edge distortions are caused by both electrostatic fluctuation and band-gap fluctuations, the resulting distortion depth γ is given by: $\gamma^2 = \gamma_{el}^2 + \gamma_{bg}^2$, which gives the following dependency versus the PL intensity:

$$\gamma = \left\{\gamma_{el,0}^2\left(\frac{I_{pl}^0}{I_{pl} + I_{pl}^0}\right)^{\frac{1}{3}} + \gamma_{bg}^2\right\}^{\frac{1}{2}}, \tag{2}$$

with $\gamma_{el,0} = \frac{e^2}{4\pi\varepsilon_r\varepsilon_0}N_I^{\frac{2}{3}}2^{\frac{-1}{3}}(bI_{pl}^0)^{\frac{-1}{6}}$ the electrostatic fluctuation depth in

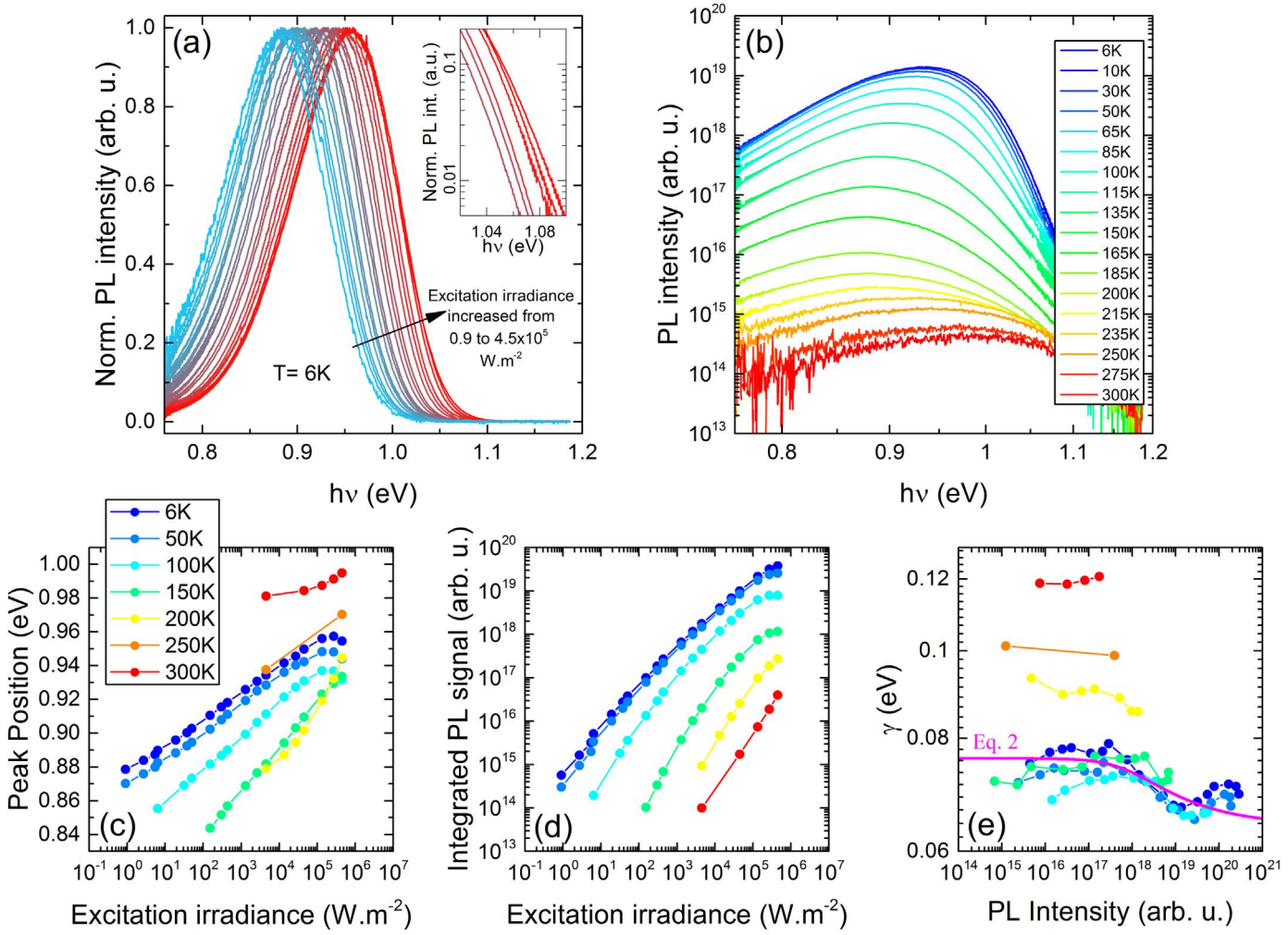

Fig. 2. Excitation and temperature-dependent PL of CZTSSe. (a) CZTSSe normalised PL spectra measured at 6 K under increased laser excitation irradiance, the insert show the change of the high energy side slope due to laser heating for the two highest excitation. (b) Semi-logarithmic plot of temperature dependent PL spectra of CZTSSe under 4500 W m^{-2} laser excitation irradiance. Peak maximum position (c) and intensity (d) plotted versus laser excitation irradiance. (e) Standard deviation of the Gaussian fit of the low energy side of the PL peak, γ, versus PL intensity. Plots (c), (d) and (e) share the same colour-coded temperature scale displayed in (c). (For interpretation of the references to color in this figure legend, the reader is referred to the web version of this article).

absence of screening from photo-generated carriers and $I_{pl}^{0} = p'^{2}/(4b)$ is the PL intensity for which the screening from photo-generated carriers starts to be dominant. In Fig. 2e, for low temperatures, the decrease in measured γ seen in the 10^{18}–10^{19} arbitrary unit range of PL intensity is attributed to the screening of the Coulombic potential of charged defects. Since the drop in γ is limited from 76 meV to 64 meV, the electrostatic fluctuations are not the main source of potential distortion in CZTSSe. The magenta line illustrates the calculated behaviour expected from Eq. (2) with $\gamma_{bg} = 64$ meV and $\gamma_{el,0} = \sqrt{76^2 - 64^2} \simeq 41$ meV, the relative contribution to γ being about 70% for the band-gap fluctuation and 30% for the electrostatic potential fluctuation, taking into account that their contributions do not add up linearly. This simple model gives a consistent, albeit qualitative, description of the data because we assumed the contribution of the band-gap variations to the PL broadening to be independent of the photogenerated carrier density. In reality, when the carrier densities increase, carriers will populate higher energy states belonging to more diverse defect configurations than the minimum energy state achievable only by a few defect configurations, which broadens the PL peak and thus increase the measured value of γ.

The laser excitation, at which the drop occurs, increases with the temperature because thermally excited carriers quickly recombine non-radiatively reducing the PL intensity. Above 150 K the transition is outside the investigated range of excitation. With temperature, γ first decreases, which is attributed to more mobile carrier being redistributed from local energy minima to deeper minima before recombination, reducing the energy range of the states involved in the PL emission. Then when thermal energy becomes important, carriers can reach higher energy states, which broadens the PL as discussed for increased excitation. Furthermore, above 150 K the contribution of both TI and TT recombination processes broadens the PL peak, leading to an increase in optically measured γ beyond the intrinsic fluctuation depth.

From the low temperature measurements we can conclude that the fluctuations are dominated by band-gap fluctuations. The question now arises about what causes these band-gap fluctuations. Since these measurements were performed on CZTSSe films, band gap fluctuations related to S-Se distribution inhomogeneities cannot be excluded; also, it appears likely that Cu-Zn disorder may still contribute to the band-gap fluctuations.

3.2. Sub-band-gap absorption of kesterite with different degree of Cu-Zn order

To clarify the sources of the band-gap fluctuations and its potential link with the Cu-Zn disorder, we perform quantitative measurements of the density of states in the tails via the absorption coefficient on the same CZTSSe samples and on CZTSe samples, where S-Se distribution is

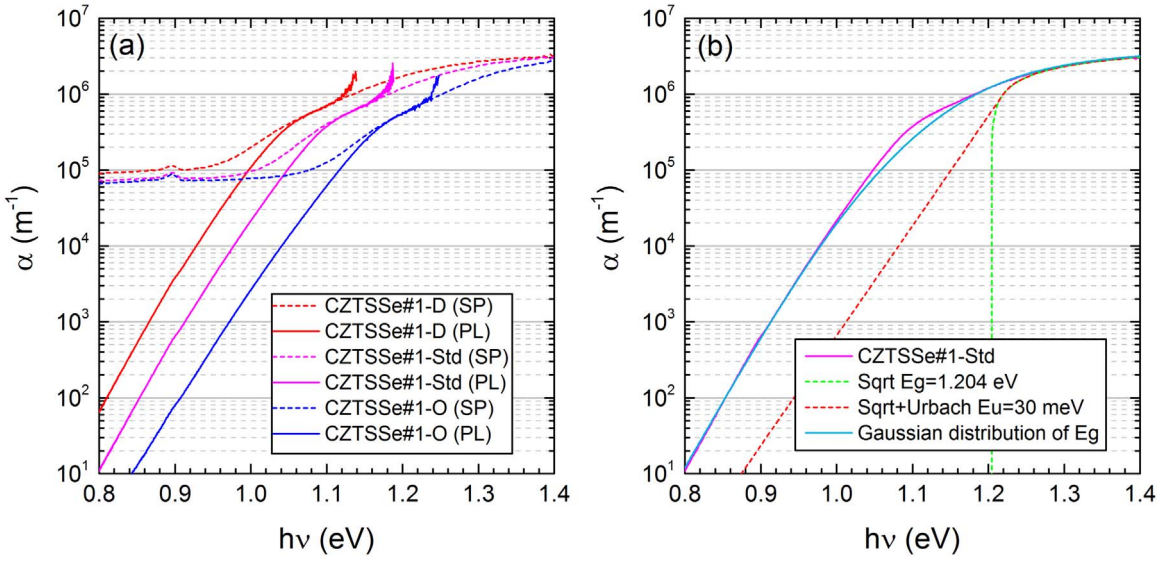

Fig. 3. (a) Absorption coefficient measured by SP and PL of sulfo-selenides kesterite with different thermal treatments inducing different Cu-Zn ordering degree of the kesterite structure (D – low, Std – intermediate, O – higher order parameter, respectively). (b) Measured absorption coefficient compared to best fits with different models. Sqrt gives the square root behaviour of the extended states for the band-gap energy Eg determined by Tauc's approach; Sqrt + Urbach shows the previous behaviour modified to include an Urbach tail (see Eq. (4)). The Gaussian curve is obtained using Eq. (3) with $\overline{E_g}$ = 1.184 eV, E_u = 25 meV and σ = 74 meV.

absent, both with varying Cu-Zn order state.

To reliably quantify the density of states over a large range and to resolve the deep band-tails, we combine PL and SP measurement of the absorption coefficient. SP has a good accuracy for high α values, but saturates below $\alpha = 10^5\ m^{-1}$ as seen in Fig. 3a due to light trapping in the thin-films. PL is very accurate in the low absorption range [47,64] and interestingly, the substrate absorption is not a limiting factor when the absorption coefficient is determined by PL. However, PL has a limited accuracy for measurement in the high absorption range since PL is emitted only from near band edge states and in the range of high absorption most of the PL signal is re-absorbed by the material itself leading to a weak PL signal.

In order to quantify the density of Cu-Zn disorder induced by [Cu_{Zn}^{-} + Zn_{Cu}^{+}] anti-site defect clusters in the Cu-Zn planes, it is useful to introduce the long range order parameter S associated with the Cu-Zn order [65], which takes the value 1 for a perfectly ordered structure and drops to 0 for a fully Cu-Zn disordered structure. The later situation is encountered when the temperature is above T_c and corresponds to a random occupation of the lattice sites in the Cu-Zn planes.

Due to the isoelectronic nature of Cu^+ and Zn^{2+} ions, S cannot be derived easily from standard XRD. Instead, neutron diffraction [31,66], nuclear magnetic resonance [32] and resonant XRD [67,68] are suitable technique for S measurement on powder samples. Raman scattering is sensitive to the change in crystal symmetry induced by the Cu-Zn disorder [36,38], whereas spectrophotometry is able to probe the band-gap energy modification resulting from the large concentration of [Cu_{Zn}^{-} + Zn_{Cu}^{+}] anti-site defect clusters [36] and both techniques have been used to derive order parameters on thin films. Recently, a direct link between band-gap energy and Cu-Zn disorder was demonstrated [69]. Here we use the band-gap energy as an order parameter. The lowest band-gap energy is observed for the fully Cu-Zn disordered kesterite and the band-gap energy increases linearly with the order parameter [36,69].

When a kesterite material is brought to a fixed temperature, S will evolve towards the equilibrium curve plotted in Fig. 1, the kinetics at which the equilibrium is reached strongly depending on the temperature (see Supplementary materials of Ref. [44]). Due to the second order nature of the Cu-Zn order-disorder transition and due to the low critical temperature, it is not practically possible to reach perfect order and 0.7–0.8 is the practical limit for S, as decades would be required for further increase in S [41]. For a given chemical composition, the degree of Cu-Zn order of the kesterite structure depends solely of the thermal history of the crystal. Here we change this parameter either by post-deposition annealing in nitrogen atmosphere followed by thermal quenching or by changing the rate of the cooling from the annealing step temperature to room temperature during the final step of the sample preparation.

The absorption spectra of CZTSSe layers are plotted in Fig. 3a, where the effects of Cu-Zn order-disorder on the optical property of the kesterite are depicted. Standard CZTSSe (Std) underwent a final cool-down in 20 min from 550 °C to 180 °C and in 20 min from 180 °C to 80 °C and then a natural cool-down to room temperature; this fast cool-down in the low temperature range (below the critical temperature of the Cu-Zn disorder) will establish a low degree of Cu-Zn order. The disordered CZTSSe (D) was synthesised using the standard cooling subsequently followed by an annealing at 300 °C, above the critical temperature, to induce complete Cu-Zn disorder. Then the sample was thermally quenched to keep the kesterite in a fully Cu-Zn disordered state. As expected from previous studies [36], the band-gap narrowing, clearly seen in Fig. 3a by a red-shift of the absorption spectrum, indicates a reduction of the Cu-Zn order parameter for the quenched sample. For the slow cooled CZTSSe (O), two extra cooling steps were added before the natural cooling to room temperature which consisted of 1 h at 180 °C followed by a controlled ramp from 180 °C to 80 °C in 10 h. The long time spent below the critical temperature allows to increase the Cu-Zn order parameter and induces a band-gap widening that can be seen in Fig. 3a by the blue-shift of the absorption spectrum of the slow-cooled sample. The band-gap energy E_g values of those samples are reported in Table 1 under sample names CZTSSe#1.

The absorption spectra exhibit an exponential rise in the low absorption range corresponding to an Urbach tail behaviour [70]. The Urbach energy E_u describes the extension of tail states below the band-gap energy and was determined from the absorption spectra by fitting $\alpha(h\nu)$ in the range of $2000 - 10^5\ m^{-1}$ in order to allow a consistent comparison between samples. Values are reported in Table 1, together with the data for CZTSSe#2 samples, which were prepared with slightly less Sn than CZTSSe#1.

A similar approach was conducted on pure selenide kesterite CZTSe (CZTSe#1). The resulting spectra are plotted in Supplementary Fig. S2b. The thin films originating from the same co-evaporation process

Table 1
Summary of samples investigated and values extracted from absorption spectra analysis: band-gap energy E_g, Urbach energy E_u and standard deviation of the Gaussian distribution of band-gap energy σ. Samples with a low degree of Cu-Zn order are printed in red, samples with high degree of Cu-Zn order are printed in blue and those with an intermediate degree of Cu-Zn order are printed in black.

Material	Sample	Thermal treatment	E_g eV	E_u meV	σ meV
CZTSSe	#1-D	1 h at 300°C + quench to RT	1.162	29	76
CZTSSe	#1-Std	none	1.204	30	74
CZTSSe	#1-O	1 h at 180°C + 180→80°C in 10 h	1.264	32	77
CZTSSe	#2-D	1 h at 300°C + quench to RT	1.148	30	77
CZTSSe	#2-Std	none	1.255	30	87
CZTSSe	#2-O	1 h at 180°C + 180→80°C in 10 h	1.301	31	85
CZTSSe	#3-D	1 h at 300°C + quench to RT	1.109	28	68
CZTSSe	#3-O	3 h at 170°C + 170→100°C in 3 d + 28 d at 100°C	1.238	29	70
CZTSe	#1-D	1 h at 250°C + quench to RT	0.916	26	49
CZTSe	#1-O+D	3 d at 100°C +1 h at 250°C + quench to RT	0.913	26	49
CZTSe	#1-Std	none	0.931	25	49
CZTSe	#1-O	3 d at 100°C	0.959	27	49
CZTSe	#1-D+O	1 h at 250°C + quench to RT + 3 d at 100°C	0.959	25	49
CZTSe	#2-D	1 h at 300°C + quench to RT	0.894	28	56
CZTSe	#2-O	3 h at 170°C + 170→100°C in 3 d + 28 d at 100°C	0.952	29	59

corresponding to the as-grown sample (Std) underwent two types of annealing [44]. Ordering treatment (O) consists of an annealing at 100 °C for 3 days to promote an increase of the Cu-Zn order parameter, resulting in partial Cu-Zn ordering with a parameter of $S \simeq 0.75$ (see below). Disordering treatment (D) consists of an annealing at 250 °C for 1 h, above the CZTSe critical temperature, followed by a quenching resulting in a completely Cu-Zn disordered kesterite. The changes in band-gap energy induced by the post-synthesis annealing are reported in Table 1. Besides the expected trend in band-gap energy (that reflects the order parameter) for D and O treatment, one can see that combination of those treatments (D + O and O + D) leads to the same band-gap energy (O and D respectively) because the Cu-Zn order-disorder transition is fully reversible. The Urbach energy reported in Table 1 for CZTSe samples were extracted for α in the range of $10^4 - 10^5\ m^{-1}$.

To access quantitatively to the thermally induced change in S, annealing at 100 °C was performed for 28 days on both CZTSe#2-O and CZTSSe#3-O. The absorption spectra of those samples and their Cu-Zn disordered counterparts (CZTSe#2-D and CZTSSe#3-D, respectively) are plotted in Supplementary Fig. S2c and the corresponding E_u are reported in Table 1. Here we consider only the order parameter associated with the $[Cu_{Zn}^{-} + Zn_{Cu}^{+}]$ defect clusters, while the order parameter of the Cu-Zn planes also depends of the stoichiometry [71]. Under this assumption, the value of S reached under equilibrium depends only on the ratio of the temperature of the material and its critical temperature T_c as depicted in Fig. 1. Thus S can be easily quantified when the critical temperature is known and when the material is equilibrated at a given temperature, which is the case after the long annealing, according to the ordering kinetics parameters reported on Ref. [36]. The long range Cu-Zn order parameter was calculated to be $S = 0.73$ and $S = 0.77$ for CZTSe and CZTSSe (assuming that T_c follows the S/Se ratio linearly) respectively.

In order to give a complete picture of the densities of state, the shallow tails were also quantified. In Fig. 3b we compare the absorption spectrum to a model which combines the square root behaviour of the extended band states with an Urbach tail. One most noticeable feature of the kesterite absorption spectra is that they cannot be modelled properly by the simple combination of an Urbach behaviour below the band-energy and a square root behaviour above the band-gap energy determined from Tauc's plot for a direct semiconductor. As depicted in Fig. 3b, such approach would lead to an erroneous description of the low absorption part and the near band-gap energy region, the measured spectrum being red-shifted by 80–100 meV with respect to the modelled spectrum. Instead, a better description of the spectrum can be given by considering a Gaussian distribution of band-gap energies being centred at $\overline{E_g}$ and characterised by a standard deviation σ [27]. The absorption coefficient is derived from the absorption spectrum obtained for a unique band-gap $\alpha_0(h\nu, E_g)$:

$$\alpha = \int_0^\infty \frac{1}{\sqrt{2\sigma}} \exp\left(\frac{-(E_g - \overline{E_g})^2}{2\sigma^2}\right) \alpha_0(h\nu, E_g)\, dE_g. \tag{3}$$

Here we consider a square root behaviour for $h\nu > aE_g$ and an Urbach behaviour for $h\nu < aE_g$ with aE_g the energy where the two regimes merge:

$$\alpha_0(h\nu, E_g) = A\left[\mathscr{H}(aE_g)\frac{\sqrt{h\nu - E_g}}{E_g} + \mathscr{H}(-aE_g)\frac{\sqrt{a-1}}{a\sqrt{E_g}} e^{\frac{h\nu - aE_g}{E_u}}\right], \tag{4}$$

with A being the amplitude, $\mathscr{H}$ the Heaviside function. The Gaussian distribution of band-gap energies arises from spatially fluctuating band-gaps as determined from the temperature dependent PL measurements. The standard deviation σ of the distribution is reported in Table 1 and fits performed with Eqs. (3) and (4) are plotted in Fig. S2d. It reflects the average energy depth of the fluctuation and is in good agreement with the values of γ obtained from cold PL measurements. σ is mostly influenced by the absorption due to shallow tails, while E_u is mostly influenced from the absorption related to deep tails. Although the Gaussian distribution of band-gap energies can fit satisfactory the low and high absorption range of the spectrum, an additional contribution to α is visible in Fig. 3b around 100 meV below the band-gap energy, that could be attributed to a defect related absorption. The defect signature is quite broad since the specific energy distribution of the defect is convoluted with the distribution of band edge energies.

The presence of the band distortions and defects considerably rise the absorption coefficient below the band-gap energy and thus are responsible for the strong red-shift of the room temperature PL with respect to the band-gap energy reported in record solar cells, which limits the open-circuit voltage of the devices [16,72].

4. Discussion

The PL responses after change in excitation or temperature (Fig. 2a–d) are characteristic of semiconductors with energy levels that strongly fluctuate at microscale. The analysis of the low energy side of the PL peak (Fig. 2e), shows that the fluctuations arise from energy level distortions caused by variations in the band-gap accounting for about 70% and from electrostatic potential fluctuations accounting for about 30%. We should emphasise that this ratio is determined at low temperature. For working conditions of a solar cell, the electrostatic potential fluctuations is predicted, by Eq. (1), to be reduced because of the additional screening from thermally activated carriers and photogenerated carriers. Since the band-gap energy around or above 1 eV is large compared to the thermal energy at room temperature and since minority carrier life time decreases with increasing temperature, the establishment of a significant photogenerated carrier density under unconcentrated solar radiation is impeded. Thus such additional screening is marginal and the electrostatic fluctuation depth measured at low temperature and low-to-medium illumination reflect the value that would be measured under solar cell operation. Reasonably assuming that the higher band-gap and the lower band-gap regions show similar thermal behaviour of the band-gap energy from 150 K to 300 K, the band-gap fluctuation depth would not be significantly affected. The rise in γ seen for $T \geq 150$ K is attributed to the significant contribution of both TI and TT transitions to the PL signal leading to additional broadening. It is therefore concluded that the large band-tailing of kesterite results mainly (70%) from spatial fluctuations of the band-gap. The impact of the electrostatic potential fluctuations is lower(30%).

Comparing the Urbach energy E_u or fluctuation depth σ (Table 1) of the as-prepared material to their intentionally Cu-Zn disordered and Cu-Zn ordered material counterparts, one can conclude that changing Cu-Zn ordering by post-synthesis annealing does neither influence the Urbach energy nor the fluctuation depth. Indeed, if the band-gap energy was shifted by up to 150 meV after thermal treatment, the Urbach energy was only changed within error by 3 meV at most, without showing any trend with the band-gap energy that shows the variation of the Cu-Zn order parameter. The values of σ, reported in Table 1, measured on samples with different degrees of Cu-Zn order show that they are not influenced by the degree of Cu-Zn order in the experimentally accessible range between 0% and 80%, in agreement with recent measurement by PL emission spectroscopy [73].

Due to the second order nature of the Cu-Zn disorder transition and its low critical temperature, it is not practically possible to reach a degree of Cu-Zn order near $S = 1$ and one may argue that residual Cu-Zn disorder could hinder reduction of the Urbach energy or fluctuation depth. However, the Cu-Zn order parameter S changes from 0% to ~ 80% by the post-synthesis treatments; this corresponds to a change from one $[Cu_{Zn}^{-} + Zn_{Cu}^{+}]$ antisite defect cluster per unit cell to 0.22 antisite defect cluster per unit cell. Such 4.4 times drop of the Cu-Zn disorder related defect density would be reflected in the absorption spectrum (Urbach energy or fluctuation depth) if those defects were the main source of band tails in kesterite. Interestingly, the band-gap energy decrease induced by $[Cu_{Zn}^{-} + Zn_{Cu}^{+}]$ antisite defect clusters depends strongly on the defects arrangement and it has been theoretically calculated that the configurations leading to the largest band-gap energy decrease are the ones with the largest formation energy [39]. Accordingly, during Cu-Zn ordering, thermodynamics would promote the annihilation of the defect configurations which induce the most severe band-gap energy deviation, thus reducing the spread of band-gap distribution, which would be reflected in the absorption spectrum even after partial Cu-Zn ordering. Another suspected detrimental effect of the Cu-Zn disorder is the formation of domains with different band-gap energy for partially ordered kesterite with low order parameter S, because of the nucleation and growth of ordered domains in the Cu-Zn disordered material. If such phenomenon would be critical for the band tailing in kesterite, ones would predict a lower distortion width or Urbach energy for the fully Cu-Zn disordered material than for the partially ordered counterparts (as-grown samples). However, the data reported in Table 1 do not show any trend of lower tailing in Cu-Zn disordered material. In addition, contrary to first order phase transition, second order phase transition like the Cu-Zn disorder do not lead to phase segregation [74,75]. Since no change in the Urbach energy nor the band distortion width were observed in the absorption spectrum after thermally induced change of the Cu-Zn order parameter, we conclude that the Cu-Zn disorder is not the main origin of the large band tails in kesterite. This conclusion is supported by the results of the temperature and excitation dependent PL.

The electrostatic potential fluctuations originate from two sources: stoichiometric deviations leading to the formation of charged point defects which are not annihilated during Cu-Zn ordering and Cu-Zn disorder inducing $[Cu_{Zn}^{-} + Zn_{Cu}^{+}]$ antisite defect clusters in the form of the Cu_3 SnS and $CuZn_2SnS$ S-centred tetrahedral motifs segregated in nanodomains [33]. By ordering the kesterite, only part of the $[Cu_{Zn}^{-} + Zn_{Cu}^{+}]$ antisite defect clusters are annihilated, reducing the electrostatic potential fluctuations. Because the Cu-Zn ordering is partial and because stoichiometric deviations are unaffected by the Cu-Zn ordering, only a part of the electrostatic potential fluctuations is cured by Cu-Zn ordering. Since electrostatic potential fluctuations are only the smaller contributor to the level energy distortions (30%), reducing partly the electrostatic potential fluctuations by Cu-Zn ordering has little impact on the total level energy distortions. The fact that the Cu-Zn disorder is not directly the main origin of the large band tails in kesterite explains why the Cu-Zn ordering state of the kesterite has no impact neither on the red-shift of the PL maximum when compared to the band-gap energy [44], nor on the V_{oc} deficit ($E_g - qV_{oc}$) [4,44,76].

In the light of those findings we discuss the possible origin of band-gap fluctuations that are responsible for the large band-tailing in kesterite. The band-gap energy of CZTSSe depends of the S/Se ratio and therefore sulfo-selenide alloy disorder could be responsible. In Ref. [4], anionic disorder was investigated in CZTSSe samples with the same S/Se ratio by means of XRD and STEM and its impact on band-gap energy fluctuation was evaluated to be $\sigma = 28$ meV, which is quite far from our optically measured value reported in Table 1, especially when considering the convolution rule of Gaussian distributions. However, comparing the fluctuation width for CZTSe and CZTSSe samples in Table 1, we find values between 50 and 60 meV for the pure selenide compounds and values between 70 and 90 meV for the sulfo-selenide films. This comparison clearly indicates that sulfo-selenide alloy disorder does play a role and increases the width of the band-gap distribution and the Urbach energies. Using the convolution rule of Gaussian distributions, $\sigma = 28$ meV reported in Ref. [4] for the anionic disorder will account for a part of the difference in σ seen between CZTSe and CZTSSe, the other part coming from the fact that most of the defects clusters lead to deeper fluctuation of the band-gap in CZTS than in CZTSe [25]. Still, the Urbach energy and the width of band-gap distribution are rather large even in the pure selenide kesterite.

Ab initio calculations [25] have shown that most of defect clusters with a strong impact on the band-gap energy involve tin but their occurrences are not probable due to their high formation energy. One exception is $[2Cu_{Zn}^{-} + Sn_{Zn}^{2+}]$, which is predicted to have the third lowest formation energy of kesterite defects for a wide range of growth conditions (from 0.3 to 0.6 eV) after $[Cu_{Zn}^{-} + Zn_{Cu}^{+}]$ antisite defect clusters and Cu_{Zn} antisite. $[2Cu_{Zn}^{-} + Sn_{Zn}^{2+}]$ are predicted to narrow the band-gap energy by 0.5 eV (CZTS) and 0.2 eV (CZTSe) for a concentration of around $4 \cdot 10^{20}$ cm^{-3}, whereas for the same concentration Cu-Zn disorder related defect clusters $[Cu_{Zn}^{-} + Zn_{Cu}^{+}]$ is predicted to narrow the

band-gap energy only by a few tens of meV (~ 50 meV for CZTS and ~ 20 meV for CZTSe). Thus a rather low concentration ($<10^{20}$ cm^{-3}) of randomly distributed [$2Cu_{Zn}^{-}$ + Sn_{Zn}^{2+}] could lead to band-gap fluctuation with a standard deviation in the magnitude of those reported in Table 1. Such defect concentrations are near the detection limit of neutron diffraction and therefore are not detected in diffraction studies. In such scenario, during the growth of kesterite, which occurs above T_c, the high concentration of Cu_{Zn}^{-} resulting from Cu-Zn disorder would foster the formation of [$2Cu_{Zn}^{-}$ + Sn_{Zn}^{2+}] by stabilising the Sn_{Zn}^{2+} antisite via clustering while the formation a Sn_{Zn}^{2+} antisite alone is less probable due to its higher formation energy. Reducing the Cu-Zn disorder after the kesterite formation would have a limited impact on the band-tailing as we shown here. However reducing the Cu-Zn disorder during the kesterite formation should minimise the band-tailing. Such approach can be conducted for example by appropriate Cu or Zn substitution by element showing less similarities [77]. Indeed substitution of Cu by Ag has recently shown to significantly reduce the band-tailing [78].

5. Conclusion

To summarise, we shown that the band-edge fluctuations in CZTSSe originate mainly from band-gap fluctuations as revealed by temperature and excitation-dependent PL. We measured the absorption spectra in the vicinity of the band-gap energy and in the tail range of CZTSe and CZTSSe with different degree of Cu-Zn order. The analysis of the spectra in the framework of spatially fluctuating bands shows that the Cu-Zn disorder is not directly responsible for the large tailing reported for kesterite. Accordingly, its modification by post-synthesis thermal treatment is not effective in reducing the band-tailing as shown here nor the V_{oc} deficit [4,44,76]. However, we do not exclude the involvement of the Cu-Zn disorder-related antisites in the formation of detrimental defects responsible for the large band-tailing in kesterite. We conclude that avoiding the formation of defect clusters impacting the band-gap energy, e.g. [$2Cu_{Zn}^{-}$ + Sn_{Zn}^{2+}], which could be achieved by reducing the Cu-Zn disorder during kesterite synthesis, for example by element substitution, is needed to reduce band-tailing and further improve kesterite-based solar cells.

Acknowledgement

This work was partially funded by Fond National de la Recherche (FNR) under project ODD (Grant C13/MS/5857739). T. Schuler, P. Ramoa and M. Melchiorre are acknowledged for their assistance.

Appendix A. Supplementary data

Supplementary data associated with this article can be found in the online version at http://dx.doi.org/10.1016/j.solmat.2017.11.005.

References

[1] International Energy Agency, Photovoltaics Power Systems, Tech. rep., 2016. URL ⟨http://www.iea-pvps.org/index.php?id=6&eID=dam_frontend_push&docID=3195⟩.
[2] S. Wenham, Towards highly efficient solar cells, Nat. Photonics 6 (2012) 136–137.
[3] S. Delbos, Kësterite thin films for photovoltaics: a review, EPJ Photovolt. 3 (2012) 35004 (URL ⟨http://dx.doi.org/10.1051/epjpv/2012008⟩).
[4] S. Bourdais, C. Chon, B. Delatouche, A. Jacob, G. Larramona, C. Moisan, A. Lafond, F. Donatini, G. Rey, S. Siebentritt, A. Walsh, G. Dennler, Is the Cu/Zn Disorder the Main Culprit for the Voltage Deficit in Kesterite Solar Cells? Adv. Energy Mater. 6(12). URL ⟨http://dx.doi.org/10.1002/aenm.201502276⟩.
[5] K. Ito, T. Nakazawa, Electrical and optical properties of stannite-type quaternary semiconductor thin films, Jpn. J. Appl. Phys. 27 (11R) (1988) 2094 (URL ⟨http://stacks.iop.org/1347-4065/27/i=11R/a=2094 ⟩).
[6] J. He, L. Sun, S. Chen, Y. Chen, P. Yang, J. Chu, Composition dependence of structure and optical properties of $Cu_2ZnSn(S,Se)_4$ solid solutions: an experimental study, J. Alloy. Compd. 511 (1) (2012) 129–132, http://dx.doi.org/10.1016/j.jallcom.2011.08.099 (URL ⟨http://www.sciencedirect.com/science/article/pii/S0925838811017944 ⟩).
[7] S. Levcenco, D. Dumcenco, Y. Wang, Y. Huang, C. Ho, E. Arushanov, V. Tezlevan, K. Tiong, Influence of anionic substitution on the electrolyte electroreflectance study of band edge transitions in single crystal $Cu2ZnSn(S_xSe_{1-x})_4$ solid solutions, Opt. Mater. 34 (8) (2012) 1362–1365, http://dx.doi.org/10.1016/j.optmat.2012.02.028 (URL ⟨http://www.sciencedirect.com/science/article/pii/S0925346712000997 ⟩).
[8] S. Siebentritt, S. Schorr, Kesterites-a challenging material for solar cells, Prog. Photovolt.: Res. Appl. 20 (5) (2012) 512–519, http://dx.doi.org/10.1002/pip.2156 (URL ⟨http://dx.doi.org/10.1002/pip.2156⟩).
[9] J.-S. Seol, S.-Y. Lee, J.-C. Lee, H.-D. Nam, K.-H. Kim, Electrical and optical properties of Cu_2ZnSnS_4 thin films prepared by rf magnetron sputtering process, Sol. Energy Mater. Sol. Cells 75 (1–2) (2003) 155–162, http://dx.doi.org/10.1016/S0927-0248(02)00127-7 (PVSEC, 12 Part)(II)), URL ⟨http://www.sciencedirect.com/science/article/pii/S0927024802001277 ⟩).
[10] H. Katagiri, N. Sasaguchi, S. Hando, S. Hoshino, J. Ohashi, T. Yokota, Preparation and evaluation of Cu2ZnSnS4 thin films by sulfurization of E-B evaporated precursors, Sol. Energy Mater. Sol. Cells 49 (1) (1997) 407–414, http://dx.doi.org/10.1016/S0927-0248(97)00119-0 (URL ⟨http://www.sciencedirect.com/science/article/pii/S0927024897001190 ⟩).
[11] H. Matsushita, T. Maeda, A. Katsui, T. Takizawa, Thermal analysis and synthesis from the melts of Cu-based quaternary compounds Cu-III-IV-VI_4 and Cu_2-II-IV-VI_4 (II = Zn, Cd; III = Ga, In; IV = Ge, Sn; VI = Se), J. Cryst. Growth 208 (1–4) (2000) 416–422, http://dx.doi.org/10.1016/S0022-0248(99)00468-6 (URL ⟨http://www.sciencedirect.com/science/article/pii/S0022024899004686 ⟩).
[12] R. Mainz, A. Singh, S. Levcenko, M. Klaus, C. Genzel, K.M. Ryan, T. Unold, Phase-transition-driven growth of compound semiconductor crystals from ordered metastable nanorods, Nat. Commun. 5 (2014) 3133 (URL ⟨http://dx.doi.org/10.1038/ncomms4133⟩).
[13] W. Wang, M.T. Winkler, O. Gunawan, T. Gokmen, T.K. Todorov, Y. Zhu, D.B. Mitzi, Device characteristics of CZTSSe thin-film solar cells with 12.6% efficiency, Adv. Energy Mater. 4 (7) (2014), http://dx.doi.org/10.1002/aenm.201301465 (n/a–n/a, URL ⟨http://dx.doi.org/10.1002/aenm.201301465⟩).
[14] P. Jackson, R. Wuerz, D. Hariskos, E. Lotter, W. Witte, M. Powalla, Effects of heavy alkali elements in $Cu(In,Ga)Se_2$ solar cells with efficiencies up to 22.6%, Phys. Status Solidi (RRL) - Rapid Res. Lett. 10 (8) (2016) 583–586, http://dx.doi.org/10.1002/pssr.201600199 (URL ⟨http://dx.doi.org/10.1002/pssr.201600199⟩).
[15] First Solar Press Release, First Solar Achieves Yet Another Cell Conversion Efficiency World Record, 2016 February 23. URL ⟨http://investor.firstsolar.com/releasedetail.cfm?ReleaseID=956479⟩.
[16] T. Gokmen, O. Gunawan, T.K. Todorov, D.B. Mitzi, Band tailing and efficiency limitation in kesterite solar cells, Appl. Phys. Lett. 103 (10) (2013) 103506, http://dx.doi.org/10.1063/1.4820250 (URL ⟨http://scitation.aip.org/content/aip/journal/apl/103/10/10.1063/1.4820250 ⟩).
[17] A. Polizzotti, I.L. Repins, R. Noufi, S.-H. Wei, D.B. Mitzi, The state and future prospects of kesterite photovoltaics, Energy Environ. Sci. 6 (2013) 3171–3182, http://dx.doi.org/10.1039/C3EE41781F (URL ⟨http://dx.doi.org/10.1039/C3EE41781F⟩).
[18] N. Terada, S. Yoshimoto, K. Chochi, T. Fukuyama, M. Mitsunaga, H. Tampo, H. Shibata, K. Matsubara, S. Niki, N. Sakai, T. Katou, H. Sugimoto, Characterization of electronic structure of $Cu_2ZnSn(S_xSe_{1-x})_4$ absorber layer and $CdS/Cu_2ZnSn(S_xSe_{1-x})_4$ Interfaces by in-situ photoemission and inverse photoemission spectroscopy, Thin Solid Films 582 (0) (2014) 166–170, http://dx.doi.org/10.1016/j.tsf.2014.09.037 (URL ⟨http://www.sciencedirect.com/science/article/pii/S0040609014009158 ⟩).
[19] I. Repins, J. Li, A. Kanevce, C. Perkins, K. Steirer, J. Pankow, G. Teeter, D. Kuciauskas, C. Beall, C. Dehart, J. Carapella, B. Bob, J.-S. Park, S.-H. Wei, Effects of deposition termination on $Cu_2ZnSnSe_4$ device characteristics, Thin Solid Films 582 (0) (2015) 184–187, http://dx.doi.org/10.1016/j.tsf.2014.09.028 (⟨http://www.sciencedirect.com/science/article/pii/S0040609014009067 ⟩).
[20] O. Gunawan, T.K. Todorov, D.B. Mitzi, Loss mechanisms in hydrazine-processed Cu2ZnSn(Se,S)4 solar cells, Appl. Phys. Lett. 97 (23) (2010) 233506, http://dx.doi.org/10.1063/1.3522884 (⟨http://scitation.aip.org/content/aip/journal/apl/97/23/10.1063/1.3522884 ⟩).
[21] J. Li, Y. Zhang, W. Zhao, D. Nam, H. Cheong, L. Wu, Z. Zhou, Y. Sun, Solar cells: a temporary barrier effect of the alloy layer during selenization: tailoring the thickness of $MoSe_2$ for efficient $Cu_2ZnSnSe_4$ solar cells, Adv. Energy Mater. 5 (9) (2015), http://dx.doi.org/10.1002/aenm.201570048 (n/a-n/a, URL ⟨http://dx.doi.org/10.1002/aenm.201570048⟩).
[22] J.B. Li, V. Chawla, B.M. Clemens, Investigating the role of grain boundaries in CZTS and CZTSSe thin film solar cells with scanning probe microscopy, Adv. Mater. 24 (6) (2012) 720–723, http://dx.doi.org/10.1002/adma.201103470 (URL ⟨http://dx.doi.org/10.1002/adma.201103470⟩).
[23] K. Sardashti, R. Haight, T. Gokmen, W. Wang, L.-Y. Chang, D.B. Mitzi, A.C. Kummel, Impact of nanoscale elemental distribution in high-performance kesterite solar cells, Adv. Energy Mater. 5 (2015), http://dx.doi.org/10.1002/aenm.201402180 (n/a-n/a, URL ⟨http://dx.doi.org/10.1002/aenm.201402180⟩).
[24] X. Fontané, L. Calvo-Barrio, V. Izquierdo-Roca, E. Saucedo, A. Pérez-Rodriguez, J.R. Morante, D.M. Berg, P.J. Dale, S. Siebentritt, In-depth resolved Raman scattering analysis for the identification of secondary phases: characterization of Cu2ZnSnS4 layers for solar cell applications, Appl. Phys. Lett. 98 (18) (2011) 181905, http://dx.doi.org/10.1063/1.3587614 (URL ⟨http://scitation.aip.org/content/aip/journal/apl/98/18/10.1063/1.3587614 ⟩).
[25] S. Chen, A. Walsh, X.-G. Gong, S.-H. Wei, Classification of lattice defects in the kesterite Cu_2ZnSnS_4 and $Cu_2ZnSnSe_4$ earth-abundant solar cell absorbers, Adv. Mater. 25 (11) (2013) 1522–1539 (URL ⟨http://dx.doi.org/10.1002/adma.201203146⟩).
[26] S. Siebentritt, G. Rey, A. Finger, J. Sendler, T. Weiss, D. Regesch, T. Bertram, What

is the bandgap of kesterite? Sol. Energy Mater. Sol. Cells 158 (2016) 126–129, http://dx.doi.org/10.1016/j.solmat.2015.10.017 (URL <http://www.sciencedirect.com/science/article/pii/S0927024815005280 >).

[27] J. Mattheis, U. Rau, J.H. Werner, Light absorption and emission in semiconductors with band gap fluctuations – a study on Cu(In,Ga)Se_2 thin films, J. Appl. Phys. 101 (11) (2007) 113519, http://dx.doi.org/10.1063/1.2721768 (URL <http://scitation.aip.org/content/aip/journal/jap/101/11/10.1063/1.2721768 >).

[28] T. Walter, R. Herberholz, C. Müller, H.W. Schock, Determination of defect distributions from admittance measurements and application to Cu(In,Ga)Se_2 based heterojunctions, J. Appl. Phys. 80 (8) (1996) 4411–4420, http://dx.doi.org/10.1063/1.363401 (URL <http://scitation.aip.org/content/aip/journal/jap/80/8/10.1063/1.363401 >).

[29] U. Rau, H. Schock, Electronic properties of Cu(In,Ga)Se_2 heterojunction solar cells-recent achievements, current understanding, and future challenges, Appl. Phys. A 69 (2) (1999) 131–147, http://dx.doi.org/10.1007/s003390050984 (URL <http://dx.doi.org/10.1007/s003390050984>).

[30] J.H. Werner, J. Mattheis, U. Rau, Efficiency limitations of polycrystalline thin film solar cells: case of Cu(In,Ga)Se2, Thin Solid Films 480–481 (2005) 399–409, http://dx.doi.org/10.1016/j.tsf.2004.11.052 (EMRS, 2004 Proceedings of Symposium O on Thin Film Chalcogenide Photovoltaic Materials,)EMRS, 2004 Conference, Strasbourg, France, May 24–28, 2004) URL <http://www.sciencedirect.com/science/article/pii/S0040609004016128 >).

[31] S. Schorr, The crystal structure of kesterite type compounds: a neutron and X-ray diffraction study, Sol. Energy Mater. Sol. Cells 95 (6) (2011) 1482–1488 (URL <http://www.sciencedirect.com/science/article/pii/S0927024811000031 >).

[32] L. Choubrac, M. Paris, A. Lafond, C. Guillot-Deudon, X. Rocquefelte, S. Jobic, Multinuclear 67Zn 119Sn and 65Cu NMR spectroscopy – an ideal technique to probe the cationic ordering in Cu_2ZnSnS_4 photovoltaic materials, Phys. Chem. Chem. Phys. 15 (2013) 10722–10725, http://dx.doi.org/10.1039/C3CP51320C.

[33] P. Zawadzki, A. Zakutayev, S. Lany, Entropy-driven clustering in tetrahedrally bonded multinary materials, Phys. Rev. Appl. 3 (2015) 034007, http://dx.doi.org/10.1103/PhysRevApplied.3.034007 (URL <http://link.aps.org/doi/10.1103/PhysRevApplied.3.034007 >).

[34] J. Paier, R. Asahi, A. Nagoya, G. Kresse, Cu_2ZnSnS_4 as a potential photovoltaic material: a hybrid Hartree-Fock density functional theory study, Phys. Rev. B 79 (2009) 115126, http://dx.doi.org/10.1103/PhysRevB.79.115126 (URL <http://link.aps.org/doi/10.1103/PhysRevB.79.115126 >).

[35] D. Huang, C. Persson, Band gap change induced by defect complexes in Cu_2ZnSnS_4, Thin Solid Films 535 (0) (2013) 265–269 (URL <http://www.sciencedirect.com/science/article/pii/S004060901004 >).

[36] G. Rey, A. Redinger, J. Sendler, T.P. Weiss, M. Thevenin, M. Guennou, B. El Adib, S. Siebentritt, The band gap of Cu2ZnSnSe4: effect of order-disorder, Appl. Phys. Lett. 105 (11) (2014) 112106, http://dx.doi.org/10.1063/1.4896315 (URL <http://scitation.aip.org/content/aip/journal/apl/105/11/10.1063/1.4896315 >).

[37] C. Krammer, C. Huber, C. Zimmermann, M. Lang, T. Schnabel, T. Abzieher, E. Ahlswede, H. Kalt, M. Hetterich, Reversible order-disorder related band gap changes in $Cu_2ZnSn(S,Se)_4$ via post-annealing of solar cells measured by electroreflectance, Appl. Phys. Lett. 105 (26) (2014) 262104, http://dx.doi.org/10.1063/1.4905351 (URL <http://scitation.aip.org/content/aip/journal/apl/105/26/10.1063/1.4905351 >).

[38] J.J.S. Scragg, L. Choubrac, A. Lafond, T. Ericson, C. Platzer-Björkman, A low-temperature order-disorder transition in Cu_2ZnSnS_4 thin films, Appl. Phys. Lett. 104 (4) (2014) 041911, http://dx.doi.org/10.1063/1.4863685 (URL <http://scitation.aip.org/content/aip/journal/apl/104/4/10.1063/1.4863685 >).

[39] J.J.S. Scragg, J.K. Larsen, M. Kumar, C. Persson, J. Sendler, S. Siebentritt, C. Platzer Björkman, Cu-Zn disorder and band gap fluctuations in $Cu_2ZnSn(S,Se)_4$: theoretical and experimental investigations, Phys. Status Solidi B 253 (2015) (2015) 247–254, http://dx.doi.org/10.1002/pssb.201552530 (URL <http://dx.doi.org/10.1002/pssb.201552530>).

[40] B.G. Mendis, M.D. Shannon, M.C. Goodman, J.D. Major, R. Claridge, D.P. Halliday, K. Durose, Direct observation of Cu, Zn cation disorder in Cu2ZnSnS4 solar cell absorber material using aberration corrected scanning transmission electron microscopy, Prog. Photovolt.: Res. Appl. 22 (1) (2014) 24–34, http://dx.doi.org/10.1002/pip.2279 (URL <http://dx.doi.org/10.1002/pip.2279>).

[41] K. Rudisch, Y. Ren, C. Platzer-Björkman, J. Scragg, Order-disorder transition in B-type Cu_2ZnSnS_4 and limitations of ordering through thermal treatments, Appl. Phys. Lett. 108 (23) (2016) 231902, http://dx.doi.org/10.1063/1.4953349 (URL <http://scitation.aip.org/content/aip/journal/apl/108/23/10.1063/1.4953349 >).

[42] W.L. Bragg, E.J. Williams, The effect of thermal agitation on atomic arrangement in alloys, Proc. R. Soc. Lond. Ser. A 145 (855) (1934) 699–730, http://dx.doi.org/10.1098/rspa.1934.0132 (arXiv:145/855/699.full.pdf+html , URL <http://rspa.royalsocietypublishing.org/content/145/855/699.short >).

[43] X. Liu, Y. Feng, H. Cui, F. Liu, X. Hao, G. Conibeer, D.B. Mitzi, M. Green, The current status and future prospects of kesterite solar cells: a brief review, Prog. Photovolt.: Res. Appl. 24 (6) (2016) 879–898, http://dx.doi.org/10.1002/pip.2741 (URL <http://dx.doi.org/10.1002/pip.2741>).

[44] G. Rey, T. Weiss, J. Sendler, A. Finger, C. Spindler, F. Werner, M. Melchiorre, M. Hála, M. Guennou, S. Siebentritt, Ordering kesterite improves solar cells: a low temperature post-deposition annealing study, Sol. Energy Mater. Sol. Cells 151 (2016) 131–138, http://dx.doi.org/10.1016/j.solmat.2016.02.014 (URL <http://www.sciencedirect.com/science/article/pii/S0927024816000763 >).

[45] G. Larramona, S. Bourdais, A. Jacob, C. Chone, T. Muto, Y. Cuccaro, B. Delatouche, C. Moisan, D. Pere, G. Dennler, Efficient Cu2ZnSnS4 solar cells spray coated from a hydro-alcoholic colloid synthesized by instantaneous reaction, RSC Adv. 4 (2014) 14655–14662, http://dx.doi.org/10.1039/C4RA01707B (URL <http://dx.doi.org/10.1039/C4RA01707B>).

[46] G. Larramona, S. Bourdais, A. Jacob, C. Chon, T. Muto, Y. Cuccaro, B. Delatouche, C. Moisan, D. Pr, G. Dennler, 8.6% efficient CZTSSe solar cells sprayed from water-ethanol CZTS colloidal solutions, J. Phys. Chem. Lett. 5 (21) (2014) 3763–3767, http://dx.doi.org/10.1021/jz501864a (arXiv:10.1021/jz501864a , URL <http://dx.doi.org/10.1021/jz501864a>).

[47] E. Daub, P. Würfel, Ultralow values of the absorption coefficient of Si obtained from luminescence, Phys. Rev. Lett. 74 (1995) 1020–1023, http://dx.doi.org/10.1103/PhysRevLett.74.1020 (URL <http://link.aps.org/doi/10.1103/PhysRevLett.74.1020 >).

[48] M. Oueslati, M. Zouaghi, M.E. Pistol, L. Samuelson, H.G. Grimmeiss, M. Balkanski, Photoluminescence study of localization effects induced by the fluctuating random alloy potential in indirect band-gap $GaAs_{1-x}P_x$, Phys. Rev. B 32 (1985) 8220–8227, http://dx.doi.org/10.1103/PhysRevB.32.8220 (URL <http://link.aps.org/doi/10.1103/PhysRevB.32.8220 >).

[49] P.W. Yu, Excitation dependent emission in Mg, Be, Cd, and Zn implanted GaAs, J. Appl. Phys. 48 (12) (1977) 5043–5051, http://dx.doi.org/10.1063/1.323631 (http://scitation.aip.org/content/aip/journal/jap/48/12/10.1063/1.323631).

[50] I. Dirnstorfer, M. Wagner, D.M. Hofmann, M.D. Lampert, F. Karg, B.K. Meyer, Characterization of CuIn(Ga)Se2 thin films, Phys. Status Solidi A 168 (1) (1998) 163–175, http://dx.doi.org/10.1002/(SICI)1521-396X(199807)168:1<163::AID-PSSA163>3.0.CO;2-T (URL <http://dx.doi.org/10.1002/(SICI)1521-396X(199807)168:1163::AID-PSSA1633.0.CO;2-T>.

[51] S. Siebentritt, Wide Gap Chalcopyrites, Springer, Berlin, Heidelberg, New York, 2006.

[52] T. Gershon, B. Shin, N. Bojarczuk, T. Gokmen, S. Lu, S. Guha, Photoluminescence characterization of a high-efficiency Cu2ZnSnS4 device, J. Appl. Phys. 114 (15) (2013) 154905, http://dx.doi.org/10.1063/1.4825317 (arXiv:10.1063/1.4825317 , URL <http://dx.doi.org/10.1063/1.4825317>).

[53] M.J. Romero, H. Du, G. Teeter, Y. Yan, M.M. Al-Jassim, Comparative study of the luminescence and intrinsic point defects in the kesterite Cu_2ZnSnS_4 and chalcopyrite Cu(In,Ga)Se_2 thin films used in photovoltaic applications, Phys. Rev. B 84 (2011) 165324, http://dx.doi.org/10.1103/PhysRevB.84.165324 (URL <http://link.aps.org/doi/10.1103/PhysRevB.84.165324 >).

[54] D.P. Halliday, R. Claridge, M.C.J. Goodman, B.G. Mendis, K. Durose, J.D. Major, Luminescence of Cu2ZnSnS4 polycrystals described by the fluctuating potential model, J. Appl. Phys. 113 (22) (2013) 223503, http://dx.doi.org/10.1063/1.4810846 (arXiv:10.1063/1.4810846 , URL <http://dx.doi.org/10.1063/1.4810846>).

[55] M.V. Yakushev, J. Márquez-Prieto, I. Forbes, P.R. Edwards, V.D. Zhivulko, A.V. Mudryi, J. Krustok, R.W. Martin, Radiative recombination in Cu2ZnSnSe4 thin films with Cu deficiency and Zn excess, J. Phys. D: Appl. Phys. 48 (47) (2015) 475109 (URL <http://stacks.iop.org/0022-3727/48/i=47/a=475109 >).

[56] J. Márquez-Prieto, M. Yakushev, I. Forbes, J. Krustok, P. Edwards, V. Zhivulko, O. Borodavchenko, A. Mudryi, M. Dimitrievska, V. Izquerdo-Roca, N. Pearsall, R. Martin, Impact of the selenisation temperature on the structural and optical properties of {CZTSe} absorbers, Sol. Energy Mater. Sol. Cells 152 (2016) 42–50, http://dx.doi.org/10.1016/j.solmat.2016.03.018 (URL <http://www.sciencedirect.com/science/article/pii/S0927024816001203 >).

[57] N. Wieser, O. Ambacher, H.-P. Felsl, L. Görgens, M. Stutzmann, Compositional fluctuations in GaInN/GaN double heterostructures investigated by selectively excited photoluminescence and Raman spectroscopy, Appl. Phys. Lett. 74 (26) (1999) 3981–3983, http://dx.doi.org/10.1063/1.124243 (URL <http://scitation.aip.org/content/aip/journal/apl/74/26/10.1063/1.124243 >).

[58] W. Grieshaber, E.F. Schubert, I.D. Goepfert, R.F. Karlicek, M.J. Schurman, C. Tran, Competition between band gap and yellow luminescence in GaN and its relevance for optoelectronic devices, J. Appl. Phys. 80 (8) (1996) 4615–4620, http://dx.doi.org/10.1063/1.363443 (URL <http://scitation.aip.org/content/aip/journal/jap/80/8/10.1063/1.363443 >).

[59] C. Spindler, D. Regesch, S. Siebentritt, Revisiting radiative deep-level transitions in CuGaSe2 by photoluminescence, Appl. Phys. Lett. 109 (3) (2016) 032105, http://dx.doi.org/10.1063/1.4959557 (URL <http://scitation.aip.org/content/aip/journal/apl/109/3/10.1063/1.4959557 >).

[60] S. Levcenko, J. Just, A. Redinger, G. Larramona, S. Bourdais, G. Dennler, A. Jacob, T. Unold, Deep defects in $Cu_2Sn(S, Se)_4$ solar cells with varying Se content, Phys. Rev. Appl. 5 (2016) 024004, http://dx.doi.org/10.1103/PhysRevApplied.5.024004 (URL <http://link.aps.org/doi/10.1103/PhysRevApplied.5.024004 >).

[61] E.O. Kane, Thomas-Fermi approach to impure semiconductor band structure, Phys. Rev. 131 (1963) 79–88, http://dx.doi.org/10.1103/PhysRev.131.79 (URL <http://link.aps.org/doi/10.1103/PhysRev.131.79 >).

[62] A.P. Levanyuk, V.V. Osipov, Edge luminescence of direct-gap semiconductors, Sov. Phys. Uspekhi 24 (3) (1981) 187 (URL <http://stacks.iop.org/0038-5670/24/i=3/a=R02 >).

[63] S. Siebentritt, N. Papathanasiou, M. Lux-Steiner, Potential fluctuations in compensated chalcopyrites, Phys. B: Condens. Matter 376377 (2006) 831–833, http://dx.doi.org/10.1016/j.physb.2005.12.208 (Proceedings of the 23rd International Conference on Defects in Semiconductors, URL <http://www.sciencedirect.com/science/article/pii/S0921452605015966 >).

[64] G. Rey, C. Spindler, S. Siebentritt, N. M., R. Carius, S. Li, C. Platzer-Björkman, Absorption Coefficient of Semiconductor Thin-film: Measurement from Photoluminescence, 2017, Submitted for publication.

[65] G.H. Vineyard, Theory of order-disorder kinetics, Phys. Rev. 102 (1956) 981–992, http://dx.doi.org/10.1103/PhysRev.102.981 (URL <http://link.aps.org/doi/10.1103/PhysRev.102.981 >).

[66] A. Ritscher, M. Hoelzel, M. Lerch, The order-disorder transition in Cu2ZnSnS4 – a neutron scattering investigation, J. Solid State Chem. 238 (2016) 68–73, http://dx.doi.org/10.1016/j.jssc.2016.03.013 (URL <http://www.sciencedirect.com/

science/article/pii/S0022459616300846 ›).

[67] A. Lafond, L. Choubrac, C. Guillot-Deudon, P. Fertey, M. Evain, S. Jobic, X-ray resonant single-crystal diffraction technique, a powerful tool to investigate the kesterite structure of the photovoltaic Cu2ZnSnS4 compound, Acta Crystallogr. Sect. B 70 (2) (2014) 390–394, http://dx.doi.org/10.1107/S2052520614003138.

[68] K.H. Stone, S.T. Christensen, S.P. Harvey, G. Teeter, I.L. Repins, M.F. Toney, Quantifying point defects in Cu2ZnSn(S,Se)4 thin films using resonant x-ray diffraction, Appl. Phys. Lett. 109 (16) (2016) 161901, http://dx.doi.org/10.1063/1.4964738 (URL ‹http://scitation.aip.org/content/aip/journal/apl/109/16/10.1063/1.4964738 ›).

[69] D.M. Többens, G. Gurieva, S. Levcenko, T. Unold, S. Schorr, Temperature dependency of Cu/Zn ordering in CZTSe kesterites determined by anomalous diffraction, Phys. Status Solidi B 253 (2016) 1890–1897, http://dx.doi.org/10.1002/pssb.201600372 (URL ‹http://dx.doi.org/10.1002/pssb.201600372›).

[70] F. Urbach, The long-wavelength edge of photographic sensitivity and of the electronic absorption of solids, Phys. Rev. 92 (1953) 1324, http://dx.doi.org/10.1103/PhysRev.92.1324 (URL ‹http://link.aps.org/doi/10.1103/PhysRev.92.1324 ›).

[71] M. Valentini, C. Malerba, F. Menchini, D. Tedeschi, A. Polimeni, M. Capizzi, A. Mittiga, Effect of the order-disorder transition on the optical properties of Cu2ZnSnS4, Appl. Phys. Lett. 108 (21) (2016) 211909, http://dx.doi.org/10.1063/1.4952973 (arXiv:10.1063/1.4952973 , URL ‹http://dx.doi.org/10.1063/1.4952973›).

[72] S. Siebentritt, Why are kesterite solar cells not 20% efficient? Thin Solid Films 535 (0) (2013) 1–4, http://dx.doi.org/10.1016/j.tsf.2012.12.089 (URL ‹http://www.sciencedirect.com/science/article/pii/S0040609013000151 ›).

[73] M. Lang, T. Renz, N. Mathes, M. Neuwirth, T. Schnabel, H. Kalt, M. Hetterich, Influence of the Cu Content in Cu2ZnSn(S,Se)4 solar cell absorbers on order-disorder related band gap changes, Appl. Phys. Lett. 109 (14) (2016) 142103, http://dx.doi.org/10.1063/1.4964346 (URL ‹http://scitation.aip.org/content/aip/journal/apl/109/14/10.1063/1.4964346 ›).

[74] V. Šíma, Order-disorder transformations in materials, J. Alloy. Compd. 378 (1–2) (2004) 44–51, http://dx.doi.org/10.1016/j.jallcom.2003.11.166 (Proceedings of the 9th International Symposium on Physics of Materials, ISPMA 9), (URL ‹http://www.sciencedirect.com/science/article/pii/S0925838804001069 ›).

[75] L.D. Landau, E.M. Lifshitz, Statistical Physics Part 1, Pergamon Press, 1980.

[76] C. Krammer, C. Huber, A. Redinger, D. Sperber, G. Rey, S. Siebentritt, H. Kalt, M. Hetterich, Diffuse electroreflectance of thin-film solar cells: Suppression of interference-related lineshape distortions, Appl. Phys. Lett. 107(22). ‹http://dx.doi.org/10.1063/1.4936649›, URL ‹http://scitation.aip.org/content/aip/journal/apl/107/22/10.1063/1.4936649›.

[77] T. Gershon, D. Bishop, P. Antunez, S. Singh, K.W. Brew, Y.S. Lee, O. Gunawan, T. Gokmen, T. Todorov, R. Haight, Unconventional kesterites: the quest to reduce band tailing in {CZTSSe}, Current Opinion in Green and Sustainable Chemistry, 2017. ‹http://dx.doi.org/10.1016/j.cogsc.2017.01.003›, URL ‹http://www.sciencedirect.com/science/article/pii/S2452223616300797›.

[78] T. Gershon, K. Sardashti, O. Gunawan, R. Mankad, S. Singh, Y.S. Lee, J.A. Ott, A. Kummel, R. Haight, Photovoltaic Device with over 5% Efficiency Based on an n-Type $Ag_2ZnSnSe_4$ Absorber, Adv. Energy Mater. 6(22). ‹http://dx.doi.org/10.1002/aenm.201601182›.